Journal Name

ARTICLE TYPE

Cite this: DOI: 00.0000/xxxxxxxxxx

Supporting information: Optical properties of organic/inorganic perovskite microcrystals through the characterization of Fabry-Pérot resonances

Fernando Ramiro-Manzano,*[a] Rocío García-Aboal,[a] Roberto Fenollosa,[a] Stefano Biasi,[b] Isabelle Rodriguez,[a] Pedro Atienzar,[a] and Francisco Meseguer[a]

Received Date
Accepted Date

DOI: 00.0000/xxxxxxxxxx

S1. Phase and propagation losses. Complex Refractive Index

The phase and losses of a wave could be expressed in a compact way employing the complex refractive index (n_c) as follows:

$$e^{ik_0 x n_c} = e^{-k_0 x n_i} e^{ik_0 x n_r} \quad \text{(S1)}$$

where $e^(ik_0 n_r x)$ and $e^(-k_0 n_i x)$ account for the phase and losses respectively, $n_c = n_r + in_i$ is the complex refractive index, n_r/n_i are the real/imaginary part of the refractive index, $k_0 = 2\pi/\lambda_0$ is the free space wavenumber and λ_0 the free space wavelength. In a typical light-propagation device formed by a high refractive index value dielectric thin film material in air or deposited on a low refractive index substrate, the field is mostly confined in the high-refractive index material, and guided by total internal reflection. Neither the phase nor the losses could be expressed directly by the refractive index of the core, because part of the light is propagated via the evanescent field in the surrounding media. The phase is related to an effective refractive index n_{eff}, defining the propagation constant $\beta = 2\pi n_{eff}/\lambda_0$ and the losses are usually expressed in cm^{-1} (or decibels $dB\ cm{-}1$), designed usually by α. The solutions are discrete, and are characterized by different n_{eff}, β, α and intensity profiles, which depend on the material and the geometry of the optical device. Each of these solutions or modes defines both, the light propagation as well as the resonant conditions.

In our first approximation, for simplicity, we consider a normal incident light propagating isotropically as a plane wave (with an infinite cross-section), so the form of the complex refractive index (Equation S1) of the bulk material could be used.

S2. Transmittance

Consider a plane-parallel sample, deposited on a glass surface (Figure 1). Therefore, the optical system is defined by three materials (1:substrate, 2:sample and 3:air) and two interfaces or semi-transparent dielectric mirrors (interfaces 1 and 2). In a transmittance experiment, the sample is illuminated from one side, ideally by a planar wave defined by an electric field amplitude E_{in} and a free space wavelength λ_0. The light enters into the sample by crossing the first dielectric interface (see Figure S1). As a result, the wave is affected by a transmission coefficient (t_{12}). Next, it propagates into the material of interest, experimenting a wavelength change ($\lambda_m = \lambda_0/n_r$), a phase change and an attenuation ($e^{ik_0 L n_c}$). Finally a portion of light escapes through the second dielectric interface (t_{23}) arriving to the detector, or is reflected (r_{23}). The reflected light recursively returns to the first interface, is reflected again (r_{21}) and propagates through the sample for the second time ($e^{2ik_0 L n_c}$), loosing intensity on each round trip. In fact, part of this lost light is transmitted (t_{23}) towards the detector. In summary, the light behaviour could be expressed as:

$$E_{out} = E_{in} t_{12} t_{23} e^{ik_0 L n_c} + E_{in} \Theta t_{12} t_{23} e^{ik_0 L n_c} + E_{in} \Theta^2 t_{12} t_{23} e^{ik_0 L n_c} + \ldots + E_{in} \Theta^N e^{ik_0 L n_c} + \ldots \quad \text{(S2)}$$

where Θ represents a round trip ($\Theta = r_{21} r_{23} e^{2ik_0 L n_c}$). Regrouping Equation S2 in a convenient way, Θ forms a geometrical series ($1 + \Theta + \Theta^2 + \ldots + \Theta^N + \ldots = 1/(1-\Theta)$). As a result, Equation S2 could be expressed in a compact way:

$$E_{out} = \frac{E_{in}\left(t_{12} t_{23} e^{ik_0 L n_c}\right)}{1 - \Theta} \quad \text{(S3)}$$

Assuming the tranmission and reflection coefficients as real, expanding the propagation of the round trip into its real ($a =$

10[a] *Instituto de Tecnología Química (CSIC-UPV), Universitat Politécnica de Valéncia, Av. Tarongers s/n, 46022 Valencia, Spain; E-mail: ferraman@fis.upv.es*

10[b] *Laboratorio di Nanoscienze, Dipartimento di Fisica, University of Trento, Via Sommarive 14, 38123 Povo (TN), Italia*

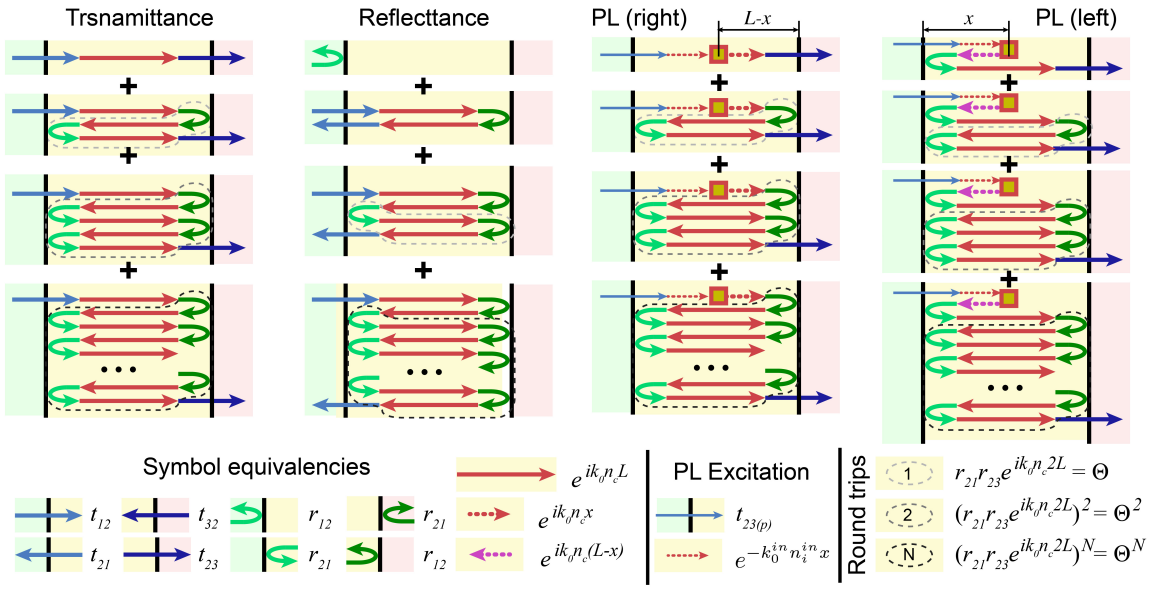

Figure S1 Scheme of light propagation in transmittance and PL.

$e^{-2k_0Ln_i}$) and immaginary parts ($b = e^{2\beta iL}$, where $\beta = k_0 n_r$), and considering the addition of the exponential with its conjugate ($b^* + b = 2cos(2\beta L)$), the Transmittance (T) takes the form of:

$$T = \left|\frac{E_{\text{out}}}{E_{\text{in}}}\right|^2 = \frac{a t_{12}^2 t_{23}^2}{a^2 r_{21}^2 r_{23}^2 - 2a r_{21} r_{23}\cos(2\beta L) + 1}, \tag{S4}$$

where t_{12}, t_{23}, r_{21} and r_{23} coefficients could be calculated by employing the Fresnel Equations. [1]

S2.1 Large transmittance and enhancement factor

The possibility of reaching full transmittance with a lossless ($a = 1$) and symmetrical cavity is mentioned in section 2.1. Here, we extend these concepts: LetâĂŹs quantify the cavity asymmetry as the ratio between reflections $y = r_{23}/r_{21}$(notice that $y = 1$ means a symmetrical cavity). Assuming lossless interfaces, $t_{ij}^2 = 1 - r_{ij}^2$, for $i, j = 1, 2, 3$, Equation 3 and 4 turn into:

$$T_{\pm,\text{lossless}} = 1 - \frac{r_{21}^2(1 \mp y)^2}{(1 \mp y r_{21}^2)^2} \tag{S5}$$

and

$$V_{lossless} = \frac{4 r_{21}^2 y}{(r_{21}^2 y + 1)^2} \tag{S6}$$

Equation S5 and S6 allow calculating the maximum transmittance T_+ and visibility V, as a function of the cavity asymmetry, y, for a lossless cavity. They confirm that full transmittance ($T_+ = 1$) is achieved for y=1, i.e. when the cavity is symmetric. As a result, the asymmetry and the absorption act as transmission penalties. In order to diminish T_- and to maximize V, the lossless and symmetry conditions should be completed with a large reflectance. Those optical devices, that accomplish these conditions, are usually known as high- or ultrahigh-quality factor resonators (see Section S7) [1]. The possibility of obtaining a high output signal (T_+) is originated by an amplified intracavity propagating wave, that travels from the source to the output interface ($I_{1\to3} = I_{out}/t_{23}^2$). The interference of this forward signal with its backward reflection ($I_{3\to1} = I_{1\to2} r_{23}^2$) results in a standing wave featured by m-number of peaks with an enhanced intensity ($I_{inside} = I_{1\to3} + I_{3\to1} + 2\sqrt{I_{1\to3} I_{3\to1}})^2$. The relation between intracavity and excitation intensity defines the peak enhancement factor (PEF),

$$PEF = \frac{(r_{23} + 1)^2 T_+}{t_{23}^2}. \tag{S7}$$

As a consequence, light-mater interactions are expected to be magnified inside the cavity, thus boosting photochemical processes such as energy harvesting [3], and photocatalysis [4]. While T_+ is symmetric for an asymmetric cavity, in the sense that it does not depend on which face (substrate/active-material active-material/air) is chosen for inserting or extracting the light, PEF is asymmetric, therefore it changes depending on the orientation of the sample. Noteworthy, the magnified output intensity produced by the amplified intracavity light fulfills energy conservation rules since the reflection spectra presents dips on one face whenever transmission peaks appear in the other face (see Section S3).

S3. Reflectance

The reflectance could be calculated in a similar way as the transmittance. Here, a determinative element is present: the reflection from the 1st interface (r_{12} see Figure S1) that is collected by the detector. This wave will interfere with the backward transmitted light (t_{21}) from the series light round-trips inside the sample. The first round-trip is composed by a single reflection, and the following contributions are equal to those of transmission ($\Theta = r_{21} r_{23} e^{2ik_0 Ln_c}$):

$$E_{out} = E_{in}\left(r_{12} + r_{23} t_{12} t_{21} e^{2ik_0 Ln_c} + r_{23} t_{12} t_{21} \Theta e^{2ik_0 Ln_c} + \ldots + r_{23} t_{12} t_{21} \Theta^N e^{2ik_0 Ln_c} + \ldots\right) \tag{S8}$$

$$E_{out} = E_{in}\left(\frac{r_{23}t_{12}t_{21}e^{2ik_0Ln_c}}{1-\Theta} + r_{12}\right) = E_{in}\frac{r_{23}(t_{12}t_{21}-r_{21}r_{23})e^{2ik_0Ln_c}+r_{12}}{1-\Theta} \tag{S9}$$

Considering lossless interfaces, the time-reversal symmetry allow us, without loss of generality, to state $t_{12}t_{21} - r_{21}r_{23} = -1$ [2]. So the Equation S9 assumes the compact form:

$$E_{out} = E_{in}\frac{r_{12} - r_{23}e^{2ik_0Ln_c}}{1-\Theta} \tag{S10}$$

and the optical reflectance (R) takes the expression,

$$R = \left|\frac{E_{out}}{E_{in}}\right|^2 = \frac{\left(a^2 r_{23}\right)^2 - 2ar_{23}r_{12}cos(2\beta L) + r_{12}^2}{a^2 r_{21}^2 r_{23}^2 - 2ar_{21}r_{23}cos(2\beta L) + 1}, \tag{S11}$$

under resonant condition ($2\beta L = 2\pi$),

$$R_{res} = \left|\frac{E_{out}}{E_{in}}\right|^2 = \left(\frac{r_{12} - ar_{23}}{1 - ar_{21}r_{23}}\right)^2 \tag{S12}$$

While the Transmittance shows a train of peaks, the reflexion spectrum shows dips. In this case, for obtaining an on-resonance null signal (the deepest dip), the numerator must be zero ($r_{12} = ar_{23}$). This is the so-called critical coupling. In this case, it can only happen when $r_{23} > r_{12}$, otherwise the optical system remains in an undercoupled regime, where the light injection underpass the lost light inside the resonator. For a symmetrical system, where $r_{12} = r_{23}$, the only possibility to obtain critical coupling is the ideal case when the material losses are neglected ($a = 1$). In summary, for obtaining the deepest reflectance dip, the glass substrate should be the exposed area to the illumination, and the uncovered surface to the detector side because the reflectance coefficient of the perovskite/air interface is higher than that of the perovskite/glass interface. The reflectance characterization is more complex than the optical transmission because of the spurious reflection of optical components as well as the coupling conditions. This is the reason why we have employed the transmittance signal in this study.

S4. PL model

The Transmission and reflection spectra of the optical system help to understand the PL model. Although the PL emission occurs inside the cavity along all directions, since our approach is one-dimensional, here we assume PL emission only in the forward and backward directions (see Figure S1). Each section of infinitesimal thickness of the sample (placed at x-distance from the first interface) is excited by the pump signal, that has lost some intensity in its way from the interface to the section. This loss is related to the exponential term ($a_{(p)x} = e^{2x - k_{0(p)}n_{i(p)}}$). Here, the addition of (p) to the subindex implies the pump signal. Therefore, in this expression, $k_{0(p)}$ corresponds to the wave number in vacuum of the excitation light and $n_{i(p)}$ corresponds to the complex part of the refractive index for such wave number. dI_{PL} of Equation S13 expresses the PL intensity emitted by the section and it can be quantified according to the generalized Planck law [5,6].

$$Id_{PL} = \frac{2k_0\xi n_i E_{hp}^2 N_{hp}}{e^{\frac{\left(E_{hp}-\mu\right)}{Tk_B}} - 1}dx, \tag{S13}$$

where E_{ph} is the energy of the emitted photons, μ is the Fermi level, k_B is the Boltzmann constant, T the temperature, dx is the thickness of the differential section, N_{ph} is the number of pumping photons, $\xi = \eta/(c^2h^3)$ includes the photogeneration efficiency η, h being the Plank constant, and c the light speed, so that $\xi \cdot N_{ph}$ allows us normalizing the PL intensity. The light emitted by a given section at the output interface can be calculated by treating it as a transmittance problem (Figure S1), where the emitted light (dI_{PL}) weighted by the loss term of the pumping signal ($a_{x(p)}$) would represent the incident light intensity ($\approx |E_{in}|^2$) for that section. This yields Equation S14 and S15 for the forward and backward emissions respectively, which are similar to Equation S4, except for terms of losses: ($a_{L-x} = e^{2-k_0n_i(L-x)}$) and ($a_{L+x} = e^{2-k_0n_i(L+x)}$) where the distance from the entering interface, x, has been taken into account, and the term $t_{12(p)}$ that corresponds to the transmittance coefficient of the pumping signal, $t_{12(p)}$ could actually be included in the normalization term $\xi \cdot N_{ph}$,

$$\text{PL-forward}, dI_{otu-f} = \frac{a_{x(p)}dI_{LP}t_{23}^2 t_{12(p)}^2 a_{L-x}}{a^2 r_{21}^2 r_{23}^2 - 2r_{23}ar_{21}\cos(2\beta L) + 1} \tag{S14}$$

$$\text{PL-backward}, dI_{otu-b} = \frac{a_{x(p)}dI_{LP}r_{21}^2 t_{23}^2 t_{12(p)}^2 a_{L+x}}{a^2 r_{21}^2 r_{23}^2 - 2ar_{21}r_{23}cos(2\beta L) + 1}. \tag{S15}$$

The PL signal emitted by the sample (Equation 6), results from the integration of the incoherent addition of S14 and S15 over L.

S5. Spectral dependencies

From a Taylor expansion of the cosine term around the resonant condition of an m-order mode and neglecting the high order terms:

$$cos(2\beta L) \approx 1 - 2L^2\left(\beta - \beta_m\right)^2 \tag{S16}$$

proceeding in a similar way with β,

$$\beta = \beta_m + \frac{d\beta}{d\lambda}\Delta\lambda, \tag{S17}$$

where

$$\frac{d\beta}{d\lambda} = k_0\frac{dn_r}{d\lambda} - \frac{\beta}{\lambda}. \tag{S18}$$

Defining the group index n_g that takes into the account the dispersion,

$$n_g = n_r - \lambda\frac{dn_r}{d\lambda}, \tag{S19}$$

then

$$\frac{d\beta}{d\lambda} = \frac{-k_0 n_g}{\lambda} \tag{S20}$$

and

$$cos(2\beta L) \approx 1 - \frac{2L^2\Delta\lambda^2 k_0^2 n_g^2}{\lambda^2}. \tag{S21}$$

Substituting the last Equation S20 into the Transmission (Equation 2) and regrouping terms, we obtain the Lorenzian form,

$$T_{peak} \approx \frac{T_+\left(\Delta\lambda_h/2\right)^2}{\left(\lambda - \lambda_r\right)^2 + \left(\Delta\lambda_h/2\right)^2} \tag{S22}$$

with a spectral broadness called Full Width at Half Maximum ($\Delta\lambda_h$)

$$\Delta\lambda_h \approx \frac{\lambda^2\,(1-ar_{21}r_{23})}{2\pi L n_g \sqrt{ar_{21}r_{23}}}. \tag{S23}$$

As expected, resonant peak features in both, the Transmittance and the PL spectra get narrower by large values of the reflection coefficients r_{ij} and low attenuation losses (large a value). Other important parameter is the distance between peaks, the so-called Free Spectral Range (FSR). In this case we consider the relation of the propagation constant between two adjacent modes:

$$\beta_{m-1} \approx \beta_m - \frac{2\pi}{2L}. \tag{S24}$$

Using Equation S17 and S20 for the Taylor series of β between β_{m-1} and β_m (assuming $\Delta\lambda \ll \lambda$), we can access $\Delta\lambda$, that permits to express the FSR as:

$$FSR = \Delta\lambda_{FSR} \approx \frac{\lambda^2}{2Ln_g} \tag{S25}$$

The parameter Finesse (F) of a resonance, is defined as the relation between the FSR and the peak broadening $\Delta\lambda_h$:

$$F = \frac{\Delta\lambda_{FSR}}{\Delta\lambda_h} \approx \frac{\pi\sqrt{ar_{21}r_{23}}}{1-ar_{21}r_{23}}, \tag{S26}$$

on another hand, it is also customary defining the quality factor Q as:

$$Q = \frac{\lambda}{\Delta\lambda_h} \approx \frac{2\pi L n_g \sqrt{ar_{21}r_{23}}}{\lambda\,(1-ar_{21}r_{23})}. \tag{S27}$$

Noteworthy, resonators with high values of both F and Q factors feature low losses and high reflectance parameters, (r_{21}, r_{23} and a tends to one). Therefore, optical features of these resonators show isolated and well separated narrow peaks in their spectra.

S6. Additional results of the fitting process

Figure S2 (a) displays fundamental optical parameters showing an increase/decrease of the ratio r_{ij}/tij $(i,j=1,2,3)$ in the proximity of the absorbance edge (where a tends to zero) due to the increase of the refractive index contrast. This can explain why those resonances with maximum values of Q and F appear around this region with relative high light confinement and moderate absorption (Figure S2 (b)). This Figure shows that PEF is asymmetric and as expected is maximized when the light enters from the most transparent interface. Noteworthy F is proportional to PEF.

S7. Analogies between resonators

The same results of this study could be obtained by applying the more compact but probably less phenomenological coupled mode theory. Such a procedure is useful when the sample presents a multilayer structure[7] with more than two interfaces. It is worth to mention that the Fabry-Pérot cavity that we have analysed above is equivalent to a Whispery Gallery Mode (WGM) resonator coupled to two waveguides, where transmittance and reflectance correspond to drop and through ports response respectively. The amplitude coefficients (t and r) are related to the coupling/transmittance coefficients (with interchanged roles, represented usually by r or k, and t respectively), the thickness of the

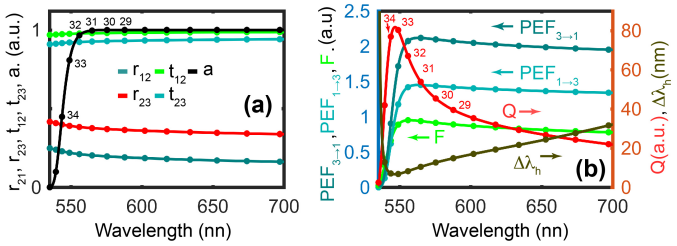

Figure S2 (a) Fundamental parameters that characterize the dielectric semi-transparent mirrors (r_{21}, r_{23}, t_{12}, t_{23}) and the term related to the absorption. (b) Resonator parameters under normal incidence/emission, derived from the fundamental optical parameters. The substrate is placed in the 2^{nd} interface. The terms of the subindex (in) and (out) of $PEF_{in\to out}$ represent the incidence and output material respectively. The dots mark the resonant positions. The series of numbers represent the m-mode order.

Fabry-Pérot cavity is equal to the round-trip length ($2L = 2\pi R$ for circular WGM resonators) and the refractive and group indexes are defined by effective values that depend on the cross section geometry and the excited propagation mode (see S1). Moreover, forcing $r_{23} = 1$ and $t_{23} = 0$ ($t_{add\to drop} = 1$ and $k_{resonator\to drop} = 0$ in a WGM cavity) the Equations become more compact and describe a simpler pass-trough WGM configuration with an only one bus-waveguide. In this way, all the Equations and concepts could be directly extrapolated to a WGM resonator with one exception: the enhancement factor is lower in a WGM resonator because of the absence of a counter-propagating wave. However, the presence of surface roughness could excite the counter propagating mode and thus the formation of a stationary wave[8], with an increased enhancement factor, similar to that of the Fabry-Pérot resonator.

S8. Material Characterization

Figure S3 shows the performed material characterization consisting in X-ray diffraction (XRD) and ultraviolet-visible spectrophotometry (UV-Vis) that corresponds to the formation of crystalline MAPbBr3 Perovskite[9].

S9. Additional data

Figure S4 displays an additional spectra of OT(a) and PL(b) of a 8.65 μ m-thick crystal. Comparing these curves to those of the sample of Fig4 (a,b), the spectral density of the ripples is clearly increased, or the FSR is diminished as expected(see 2.3). The real

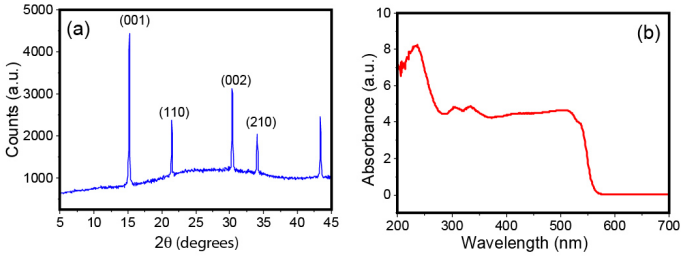

Figure S3 (a) X-ray diffraction (XRD) and (b) ultraviolet-visible spectrophotometry (UV-Vis) of the synthetized material.

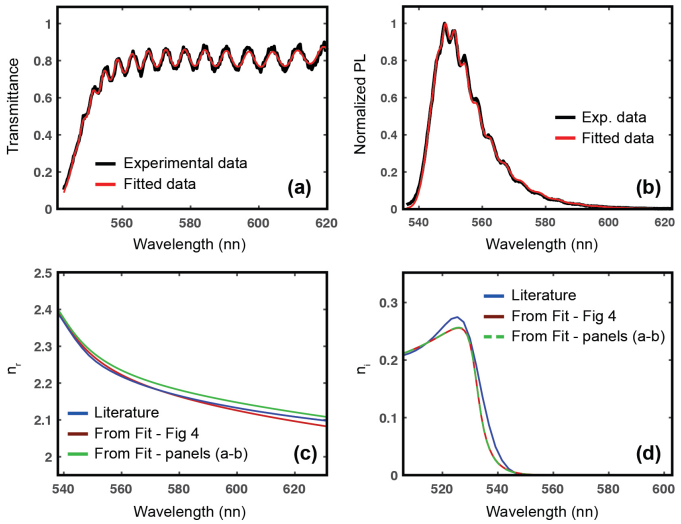

Figure S4 (a) Experimental data and (b) fitted curves for the OT and the PL spectra respectively of an additional sample. (c) Real and (d) imaginary part comparation of [11] and those extracted from the Fit of Fig 4 and pannels (a-b).

part (c) of the refractive index follows the same tendency of the imaginary part (c) for both samples. The small deviation could be due to slight differences in sample preparation, degradation as well as background and sample acquisition. In any case, the difference in the real part of the refractive index obtained from both measurements is at most around 1%, at the double fit spectral region, which is considerably smaller than the values dispersion obtained when comparing measurements from different laboratories [10].

S10. Photocarrier and Thermo-optical effects

As it is mentioned in the methods, two different light sources are employed, a blue light for acquiring the PL signal and a white source for characterizing the transmittance. As a result, one is set inside the absortion spectral region and the other covers mostly the transparent one respectively. One can think that the excited photocarriers, radiative recombination and sample temperature are different for the PL and OT experiments. This could lead to a differences in the refractive index because of excited-carrier dispersion and thermo-optical effects. Although the employed power regimes could be considered so low for observing such effects, the sample acts as a resonant cavity (with an enhancement light-matter interaction) and the material could show a giant thermo-optical coefficient (as another hybrid perovskite, $MAPbCl_3$ [12,13]). Therefore it is not possible to fully discard refractive index deviations between PL and OT experiments. In order to characterize this possible discrepancy, an additional parameter has been added to the fitting process. In particular, this new term registers the spectral deviation between curves. This results in around 0.03 nm that is below the monochromator resolution. As a result, possible refractive index discrepancies between OT and PL characterization could be considered as neglegible.

Notes and references

1 F. Ramiro-Manzano, N. Prtljaga, L. Pavesi, G. Pucker and M. Ghulinyan, *Opt. Express*, 2012, **20**, 22934–22942.

2 A. Yariv and P. Yeh, *Photonics, Optical Electronics in Modern Communications* 2007.

3 D. A. Goldman, J. Murray and J. N. Munday, *Opt. Express*, 2016, **24**, A925–A934.

4 X. Jin, J. Zhang, P. I. Morales-Guzman, J. Claverie and L. Razzari, Photonics North (PN), 2016, pp. 1–2.

5 S. Knabe, M. Langemeyer, F. Heidemann, R. Brüggemann and G. H. Bauer, *Progress in Photovoltaics: Research and Applications*, 2011, **19**.

6 O. Neumann, R. Brüggemann, N. Könne and G. H. Bauer, *physica status solidi (a)*, 2014, **211**, 1128–1133.

7 J. M. Luque-Raigon, J. Halme and H. Miguez, *Journal of Quantitative Spectroscopy and Radiative Transfer*, 2014, **134**, 9 – 20.

8 S. Biasi, F. Ramiro-Manzano, F. Turri, P. Larré, M. Ghulinyan, I. Carusotto and L. Pavesi, *IEEE Photonics Journal*, 2019, **11**, 1–14.

9 J. H. Heo, D. H. Song and S. H. Im, *Advanced Materials*, **26**, 2014, 8179–8183.

10 M. A. Martín, *Doctoral thesis, Inorganic Chemistry Department Faculty of Chemistry, University of Seville*, 2018, p. 46.

11 J.-S. Park, S. Choi, Y. Yan, Y. Yang, J. M. Luther, S.-H. Wei, P. Parilla and K. Zhu, *The Journal of Physical Chemistry Letters*, 2015, **6**, 4304–4308.

12 H. Tahara, T. Aharen, A. Wakamiya and Y. Kanemitsu, *Advanced Optical Materials*, 2018, **6**.

13 T. Handa, H. Tahara, T. Aharen and Y. Kanemitsu, *Science Advances*, 2019, **5**.